Alexandria Engineering Journal (2015) 54, 1161–1174

HOSTED BY

Alexandria University

Alexandria Engineering Journal

www.elsevier.com/locate/aej
www.sciencedirect.com

ORIGINAL ARTICLE

Comparison of DCT, SVD and BFOA based multimodal biometric watermarking systems

S. Anu H. Nair *, **P. Aruna**

Department of CSE, Annamalai University,Tamil Nadu 608002, India

Received 16 June 2014; revised 18 April 2015; accepted 4 July 2015
Available online 8 August 2015

KEYWORDS

Biometrics;
Feature extraction;
Fusion metrics;
Image fusion;
Discrete Cosine Transform (DCT);
Singular Value Decomposition (SVD) and Bacterial Foraging Optimization Algorithm (BFOA)

Abstract Digital image watermarking is a major domain for hiding the biometric information, in which the watermark data are made to be concealed inside a host image imposing imperceptible change in the picture. Due to the advance in digital image watermarking, the majority of research aims to make a reliable improvement in robustness to prevent the attack. The reversible invisible watermarking scheme is used for fingerprint and iris multimodal biometric system. A novel approach is used for fusing different biometric modalities. Individual unique modalities of fingerprint and iris biometric are extracted and fused using different fusion techniques. The performance of different fusion techniques is evaluated and the Discrete Wavelet Transform fusion method is identified as the best. Then the best fused biometric template is watermarked into a cover image. The various watermarking techniques such as the Discrete Cosine Transform (DCT), Singular Value Decomposition (SVD) and Bacterial Foraging Optimization Algorithm (BFOA) are implemented to the fused biometric feature image. Performance of watermarking systems is compared using different metrics. It is found that the watermarked images are found robust over different attacks and they are able to reverse the biometric template for Bacterial Foraging Optimization Algorithm (BFOA) watermarking technique.
© 2015 Faculty of Engineering, Alexandria University. Production and hosting by Elsevier B.V. This is an open access article under the CC BY-NC-ND license (http://creativecommons.org/licenses/by-nc-nd/4.0/).

1. Introduction

Digital watermarking is the technology of embedding information (i.e., watermark or host image) into the multimedia data (such as image, audio, video, and text), called cover image. It is realized by embedding data that it is invisible to the human visual system into a host image. Hence, the term digital image watermarking is a procedure by which watermark data are covered inside a host image which imposes imperceptible changes to the picture. Watermarking techniques have been practiced in multimodal biometric systems for the purpose of protecting and authenticating biometric data and enhancing accuracy of recognition. A multimodal biometric system combines two or more biometric data recognition results such as a combination of a subject's fingerprint, face, iris and voice. This increases the reliability of personal identification system that discriminates between an authorized person and a fraudulent person. Unimodal biometric systems depend on a single source such as a single iris or fingerprint or palmprint for authentication. It has been noticed that some of the limitations of unimodal biometric systems can be addressed by deploying

* Corresponding author. Tel.: +91 9444796816.
E-mail address: anu_jul@yahoo.co.in (S. Anu H. Nair).
Peer review under responsibility of Faculty of Engineering, Alexandria University.

http://dx.doi.org/10.1016/j.aej.2015.07.002
1110-0168 © 2015 Faculty of Engineering, Alexandria University. Production and hosting by Elsevier B.V.
This is an open access article under the CC BY-NC-ND license (http://creativecommons.org/licenses/by-nc-nd/4.0/).

multimodal biometric systems that essentially integrate the evidence submitted by multiple sources of information such as iris and palm print. Multimodal biometric system has addressed some issues related to unimodal as follows: (a) Non-universality or insufficient population coverage reduces failure to enroll rate which increases population coverage, (b) It becomes more and more unmanageable for an impostor to imitate multiple biometric traits of a legitimately enrolled individual, (c) Multimodal-biometric systems effectively address the problem of noisy data (illness affecting voice, scar affecting fingerprint).

In this paper, a multimodal biometric system has been suggested. The multimodal biometric system is implemented using different fusion schemes to improve the performance of the system. At feature extraction level the information extracted from different modalities is stored in vectors on the basis of their modality. These feature vectors are then blended to produce a joint feature vector which is the basis for the matching and recognition process. Fusion at feature extraction level generates a homogeneous template for both fingerprint and iris features. The fused image is applied as input along with the cover image to the different watermarking systems.

2. Related work

Seung-hwan et al. [1] combined numeric password along with fingerprint authentication. Here the minutia features were extracted after the fingerprint image is subjected to binarization and thinning process. Aravinth and Valarmathy [2] fused biometric features using density based score fusion. The region of interest in a fingerprint image was identified after performing binarization and thinning process. The iris pattern was encoded by Gabor filters after the process of segmentation and normalization. Kannan et al. [3] evaluated the performance of all levels of multifocused image fusion using Discrete Wavelet Transform, Stationary Wavelet Transform, Lifting Wavelet Transform, Multi Wavelet Transform, Dual Tree Discrete Wavelet Transform and Dual Tree Complex Wavelet transform in terms of various performance measures. Shah et al. [4] presented a novel fusion rule which can efficiently fuse multifocus images in the wavelet domain by taking a weighted average of the pixels. Sarup and Singhai [5] fused spatial, spectral and temporal images of the same area using PCA, Multiplicative and Wavelet HIS transformation. Among these, wavelet transform provided better results. Radha and Kavitha [6] used rank level fusion for fusing Fingerprint and Iris biometric features. Here, PCA and Fisher Linear Discriminant Methodology have been proposed for Biometric recognition. Panjeta and Sharma [7] analyzed PCA, Brovey, Wavelet and IHS fusion techniques. Maheswari et al. [8] described an innovative multimodal biometric identification system based on iris and fingerprint traits which used hamming distance based matching algorithm for calculating the hamming distance for the comparison of templates. Sahu and Parsai [9] analyzed some of the image fusion techniques for image fusion such as, primitive fusion (Averaging Method, Select Maximum, and Select Minimum), Discrete Wavelet transform based fusion, and Principal component analysis (PCA) based fusion for a set of images. Naidu and Elias [10] defined that DCT based Laplacian pyramid provided better fusion quality. Wang et al. [11] suggested a combined watermarking algorithm based on DWT, DCT and SVD which provided better robustness and impercibility. Nidalb and Adham [12] proposed a watermarking method where the cover image was decomposed by Haar transform and the watermark was converted into a stream of ones and zeroes. Tewari and Saxena [13] divided the cover image into blocks for which DCT was obtained. The watermark image was also converted into binary sequence which was embedded into the DCT blocks. Sharma et al. [14] presented an application based review of variants of BFOA that have come up with faster convergence with higher accuracy and will be useful for new researchers exploring its use in their research problems. Li et al. [15] suggested an algorithm for embedding the watermark into every 3D DC coefficient of LH and HL coefficients of each frame. This provided a PSNR value of 43.87 decibels. Khanduja et al. [16] demonstrated a novel method for watermarking relational databases for recognition and validation of ownership based on the secure embedding of blind and multi-bit watermarks using Bacterial Foraging Optimization Algorithm (BFOA). Thomas [17] provided an outline of Bacterial Foraging Optimization Algorithm (BFOA) and its intermediated operations in grid scheduling. Lenarczyk and Piotrowski [18] preferred watermark embedding and extraction in YCbCr Color model than in RGB Model. Loukhaoukha et al. [19] compressed the image using lifting wavelet transform and SVD watermarking combined with multiobjective PSO was used. Verma and Jha [20] discussed the algorithm of embedding binary watermark using CH3 subband coefficients. Liu et al. [21] developed an algorithm to embed secret image using quantization step process. Here a new performance metric Weighted Normalized Correlation was presented. Yadav and Singh [22] proposed a method to embed watermark element into a 2D DWT high entropy block.

3. Proposed work

The novel idea in this paper is the watermarking of the multimodal biometric system. This is not considered in any of the literature discussed in Section 2. In order to obtain the unique watermarked image, multimodal biometrics such as fingerprint and iris are proposed in this paper. In the proposed work which is shown in Fig. 1, fingerprint and iris biometric features are provided as input. The feature extraction procedure is performed for obtaining the distinct characteristics of fingerprint and iris. A novel approach to fuse the modalities into a watermark template is performed. Fusion techniques PCA, DWT, Laplacian pyramid and IHS are applied. The quality of fused image is assessed with respect to the fingerprint and iris images using Peak Signal to Noise Ratio (PSNR), Mean Square Error (MSE) and cross Entropy. Further, the quality of fused image is evaluated using Qabf, VIF, average gradient, edge intensity, figure definition, image entropy and mutual information (MI). Based on the quality analysis, the best fused template is identified. Then, the fused template is fed as input along with the cover image to obtain the watermarked image. Watermark embedding algorithms such as DCT, SVD and BFOA are used to embed the watermark image into the cover image. The watermark extraction algorithms such as DCT, SVD and BFOA are applied in order to elicit the hidden fused image from the cover image. The performance measures of watermarked image and the cover image are compared using PSNR, normalized cross correlation (NCC) and normalized absolute error.

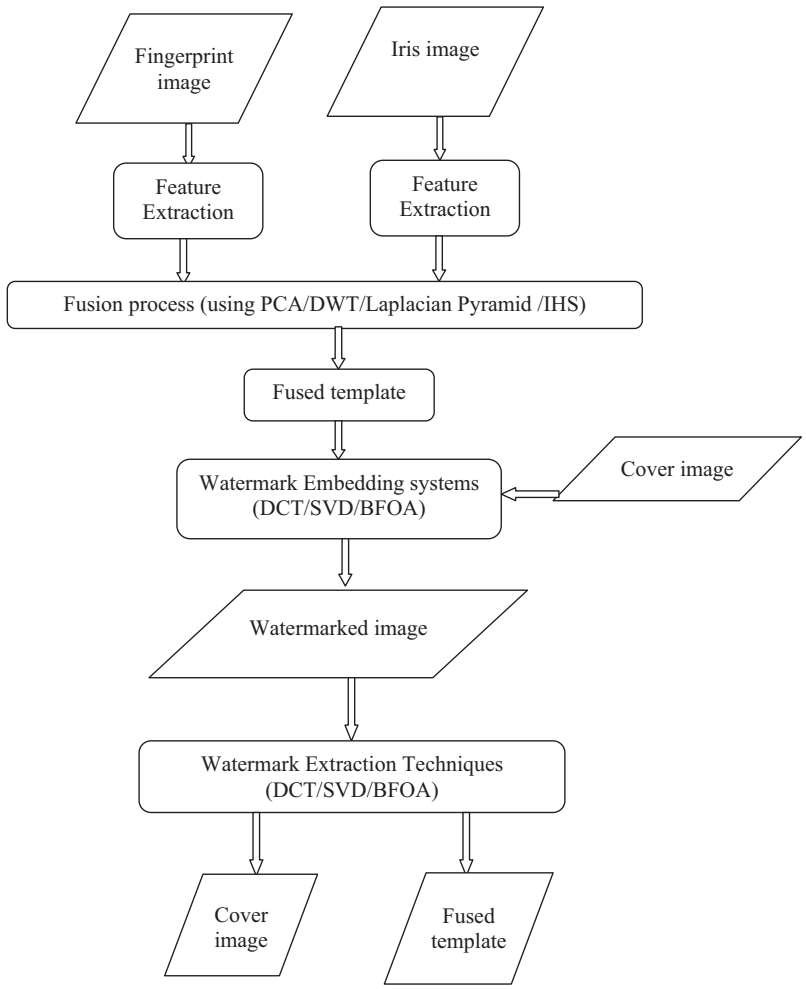

Figure 1 Flowchart of proposed work.

4. Feature extraction of fingerprint and iris

As the biometric features of fingerprint and iris are not the same, different kinds of preprocessing techniques are used for extracting the features from each one. As a first step, to enhance the image quality, pre-processing on the input image is performed. In pre-processing, the singularity region extraction process for fingerprint images and region of interest (ROI) extraction process for iris images are applied. A region of interest is a selected part of an image which can be used to perform a particular task.

4.1. Singularity region extraction from a fingerprint

After reading the fingerprint image by applying the binarization process, it is converted into binary image. It improves the contrast between the ridges and valleys in a fingerprint image. The binarized image is subjected to thinning process. Thinning is a morphological operation that erodes the foreground pixels. It preserves the connectivity of ridges.

A standard thinning algorithm that performs two subiterations is used. Each subiteration begins by examining the neighborhood of each pixel in the binary image and based on pixel-deletion criteria, and it checks whether the pixel can be deleted or not. These subiterations continue until no more pixels can be deleted. A skeletonized version of the binary image is obtained [23]. In this paper, fingerprint images of size 200×200 pixels are taken as input. The skeletonized version of the output image obtained is of size 200×200 pixels. Fig. 2 represents the flowchart for singularity region extraction from a fingerprint image.

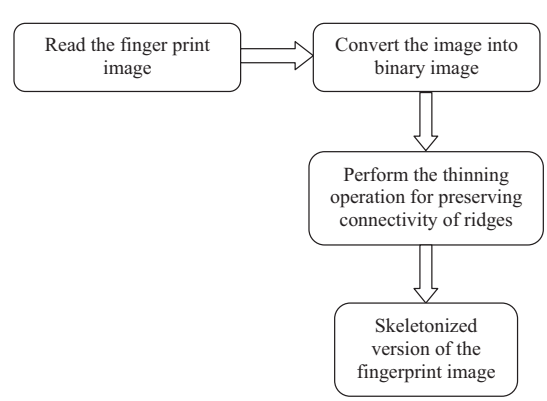

Figure 2 Flowchart for singularity region extraction from a fingerprint image.

4.2. Iris region of interest extraction

Initially, the iris image is read. Eyelids and eyelashes are considered to be 'noise' which degrades the system performance. Initially the eyelids are isolated by fitting a line to the upper and lower eyelid using the linear Hough transform [23]. First of all, the center of the iris image is found. With reference to that image center, the pupil center is found by fixing a threshold value. From the center of the pupil, the radius of the pupil is calculated. The pupil identification phase consists of two steps. The first step is an adaptive thresholding and the second step is a morphological opening operation. The first step is able to identify the pupil but it cannot eliminate the presence of noise due to the acquisition phase. The second step is performed using a structural element of circular shape. The morphological opening operation reduces the pupil area to approximate the structural element. The edge is detected using the canny edge detector by applying horizontal and vertical gradients in order to deduce edges in the image. Then, a circle is clearly present along the pupil and iris boundary. Due to the process of iris segmentation, the iris boundary is detected. The radius of the pupil is subtracted from the radius of iris to obtain the exact iris region. The iris region is in the polar pattern, which can be converted into the rectangular form for further processing. Finally, this process detects the center, radius and circumference of the pupil and the iris region even if the circumferences are usually not concentric. In this paper, Iris images of size 150×200 pixels are taken as input. The final rectangular iris image obtained is of size 64×512 pixels. Fig. 3 represents the flowchart for ROI extraction from an iris image.

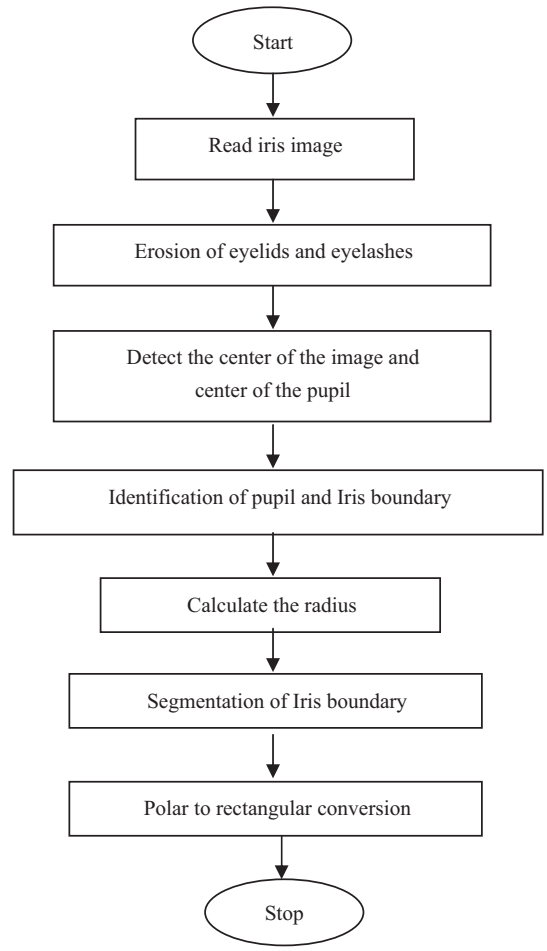

Figure 3 Flowchart for ROI extraction from an iris image.

5. Image fusion techniques

The process of image fusion is that the good information from each of the given images is fused together to form a resultant image whose quality is superior to any of the input images. In this paper, a new approach is proposed for the fusion of biometric modalities. The resultant image is the template of host image. The skeletonized version of the fingerprint image obtained is of size 200×200 pixels. The rectangular iris image obtained is of size 64×512. Both the images are resized to 512×512 pixels and they are provided as inputs to the following fusion techniques. Hence the fused output image is of size 512×512 pixels.

5.1. Fusion of fingerprint and iris using principal component analysis algorithm

Principal component analysis (PCA) is a vector space transform often used to reduce multidimensional data sets to lower dimensions for analysis. It exposes the inner structure of data in an unbiased way [24]. In this research work, the biometric modalities are given as input images. The stepwise description of the PCA algorithm for fusion is described below.

Step 1. The column vectors are generated from the input image matrices (by representing each image as a column vector).

Step 2. The mean along each column is calculated which is subtracted from each column. The column vectors form a matrix X.

Step 3. The covariance matrix of the two column vectors formed in step 1 is calculated.

$$\boldsymbol{C} = \boldsymbol{X}\boldsymbol{X}^{\boldsymbol{T}} \tag{1}$$

Step 4. The diagonal elements of the 2×2 covariance vector would contain the variance of each column vector with itself, respectively.

Step 5. The Eigenvalues and the Eigenvectors of the covariance matrix are computed.

Step 6. The column vector corresponding to the larger Eigenvalue is normalized by dividing each element with the mean of the Eigenvector.
Suppose $(x,y)^T$ is the Eigenvector corresponding to the largest eigenvalues of the images A and B, the weight values of image A and image B is as follows:

$$\boldsymbol{\omega_A} = \frac{\boldsymbol{x}}{\boldsymbol{x}+\boldsymbol{y}} \tag{2}$$

$$\boldsymbol{\omega_B} = \frac{\boldsymbol{y}}{\boldsymbol{x}+\boldsymbol{y}} \tag{3}$$

Step 7. The components of the normalized Eigenvector act as the weight values that are respectively multiplied with each pixel of the input images.

Step 8. The sum of the two scaled matrices calculated in step 6 will be the fused image matrix. Then, the fusion is accomplished using a weighted average as

$$I_F = \omega_A I_A + \omega_B I_B \tag{4}$$

where I_F is the fused image and I_A and I_B represent images A and B respectively. Fig. 4 represents the set of inputs and outputs of the fusion processing using PCA.

5.2. Fusion of fingerprint and iris using discrete wavelet transform

The discrete wavelet transform (DWT) that uses Haar wavelet allows the image decomposition in different kinds of coefficients preserving the image information. Such approximation coefficients derived from different images can be suitably combined to obtain the new coefficients which collect appropriate data from the original images. Once the coefficients are merged, the final fused image is achieved through the inverse discrete wavelet transform (IDWT), where the information in the merged coefficients is also preserved [24]. The DWT of an image x is calculated as

$$y[n] = (x * g)[n] = \sum_{k=-\alpha}^{\alpha} x[k]g[n-k] \tag{5}$$

$$y_{low}[n] = \sum_{k=-\alpha}^{\alpha} x[k]g[2n-k] \tag{6}$$

$$y_{high}[n] = \sum_{k=-\alpha}^{\alpha} x[k]h[2n-k] \tag{7}$$

where x is the input images, g is the low pass filter, h is the high pass filter and n is the number of levels. Fig. 5 represents the set of inputs and outputs of the fusion process using DWT.

5.3. Fusion of fingerprint and iris using Laplacian pyramid

An image pyramid consists of a set of low pass or band pass copies of an image, each copy representing pattern information on a different scale. At every stage of fusion using pyramid transform, the pyramid would be half the size of the pyramid from the preceding level and the higher levels will reduce upon the lower spatial frequencies. The basic idea is to construct the pyramid transform of the fused image from the pyramid transforms of the source image and then the fused image is obtained by taking inverse pyramid transform [24]. Decomposition is the process when a pyramid is generated successively at each level of the fusion. The three main steps involved in this process are as follows:

- Apply low pass filtering on input images using W = [1/16, 4/16, 6/16, 4/16, 1/16].
- Subtract the low pass filtered images and form the pyramid.
- Decimate the input image matrices by halving the number of rows and columns.

In the next step, merge the input images to form the resultant image matrix, which would be the initial input to the recomposition process. In the final step, the input image is undecimated. Undecimating the image matrix is by duplicating every row and column. The filtered matrix is merged with the pyramid formed at the level of decomposition. The merged image at the final level of recomposition will be the resultant fused image. Fig. 6 represents the set of inputs and outputs of the fusion process using Laplacian pyramid fusion.

5.4. Fusion of fingerprint and iris using IHS transform

The commonly used RGB color space is not suitable for a merging procedure, as the correlation of the image channels is not clearly emphasized. The IHS system offers certain advantage since the separate channels outline certain color properties, namely the intensity (I), hue (H), and saturation (S). This specific color space is often preferred because the visual cognitive system of human beings tends to handle the three components. The IHS coordinate system can be calculated as follows [25]:

$$\begin{bmatrix} I \\ v_1 \\ v_2 \end{bmatrix} = \begin{bmatrix} \frac{1}{\sqrt{3}} & \frac{1}{\sqrt{3}} & \frac{1}{\sqrt{3}} \\ \frac{-1}{\sqrt{6}} & \frac{-1}{\sqrt{6}} & \frac{-1}{\sqrt{6}} \\ \frac{-1}{\sqrt{2}} & \frac{-1}{\sqrt{2}} & \frac{-1}{\sqrt{2}} \end{bmatrix} \begin{bmatrix} R \\ G \\ B \end{bmatrix} \tag{8}$$

$$H = \tan^{-1} \frac{v_2}{v_1} \tag{9}$$

$$S = \sqrt{v_1^2 + v_2^2} \tag{10}$$

The corresponding inverse transform is defined as

$$v_1 = S\cos(H) \tag{11}$$

$$v_2 = S\sin(H) \tag{12}$$

$$\begin{bmatrix} R' \\ G' \\ B' \end{bmatrix} = \begin{bmatrix} \frac{1}{\sqrt{3}} & \frac{-1}{\sqrt{6}} & \frac{-1}{\sqrt{2}} \\ \frac{1}{\sqrt{3}} & \frac{-1}{\sqrt{6}} & \frac{1}{\sqrt{2}} \\ \frac{1}{\sqrt{3}} & \frac{-1}{\sqrt{6}} & 0 \end{bmatrix} \begin{bmatrix} I \\ v_1 \\ v_2 \end{bmatrix} \tag{13}$$

Fig. 7 represents the set of inputs and outputs of the fusion processing using IHS transform.

6. Image quality metrics

The performance of image fusion algorithms can be measured using the following metrics. The fused images are judged against the original source images for similarity. A number of image quality metrics have been implemented. All of these involve a reference image, which is usually the ideal fused image. However, in practice, such an ideal fused image is seldom recognized. Hence other fused image metrics such as mutual information (MI) and Petrovic and Xydeas metric have been recently proposed. These estimate the amount of information transferred from the input image to the fused image.

6.1. Xydeas and Petrovic metric – $Q^{AB/F}$

Mathematically, $Q^{AB/F}$ is defined as [26]

$$Q^{AB/F} = \frac{\sum_{m=1}^{M}\sum_{n=1}^{N}[Q^{AF}(m,n)w^A(m,n) + Q^{BF}(m,n)w^B(m,n)]}{\sum_{m=1}^{M}\sum_{n=1}^{N}[w^A(m,n) + w^B(m,n)]} \tag{14}$$

where A, B and F represent the input and fused images respectively. The definitions of Q^{AF} and Q^{BF} are same and given as

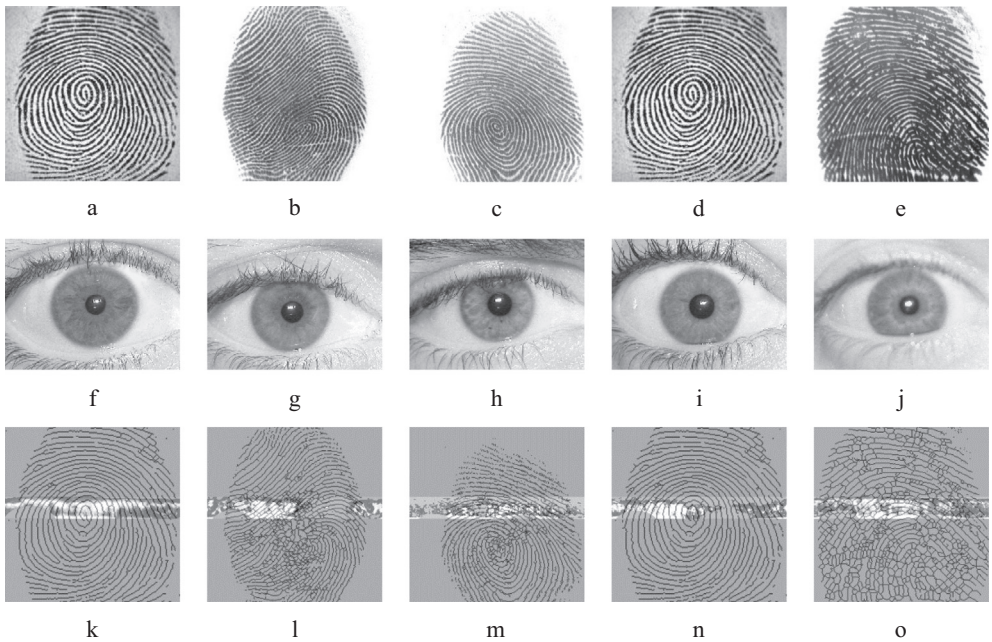

Figure 4 (a)–(e) represents input fingerprint images, (f)–(j) represents input iris images and (k)–(o) represents fused images using PCA.

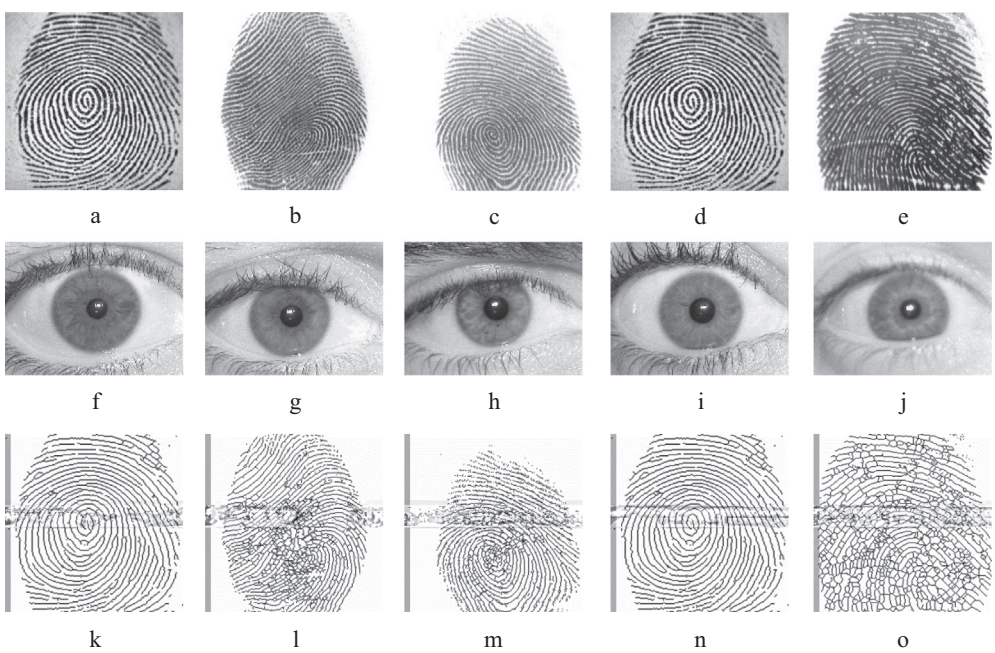

Figure 5 (a)–(e) represents input fingerprint images, (f)–(j) represents input iris images and (k)–(o) represents fused images using DWT.

$$Q^{AF}(m,n) = Q_g^{AF}(m,n) \cdot Q_\alpha^{AF}(m,n) \tag{15}$$

where Q_g^{*F} and Q_α^{*F} are the edge strength and orientation values at location (m,n) for images A and B. The dynamic range for $Q^{AB/F}$ *is* [0,1] and it should be close to one for better fusion.

6.2. Visual Information Fidelity (VIF)

VIF first decomposes the natural image into several sub-bands and parses each sub-band into blocks [27]. Then, VIF measures the visual information by computing mutual information in each block and in each sub-band. Finally, the image quality value is measured by integrating visual information for all the blocks and all the sub-bands. Image quality assessment is performed based on information fidelity where the channel imposes fundamental limits on how much information could flow from the reference image, through the image distortion process to the human observer. VIF = Distorted Image Information/Reference Image Information

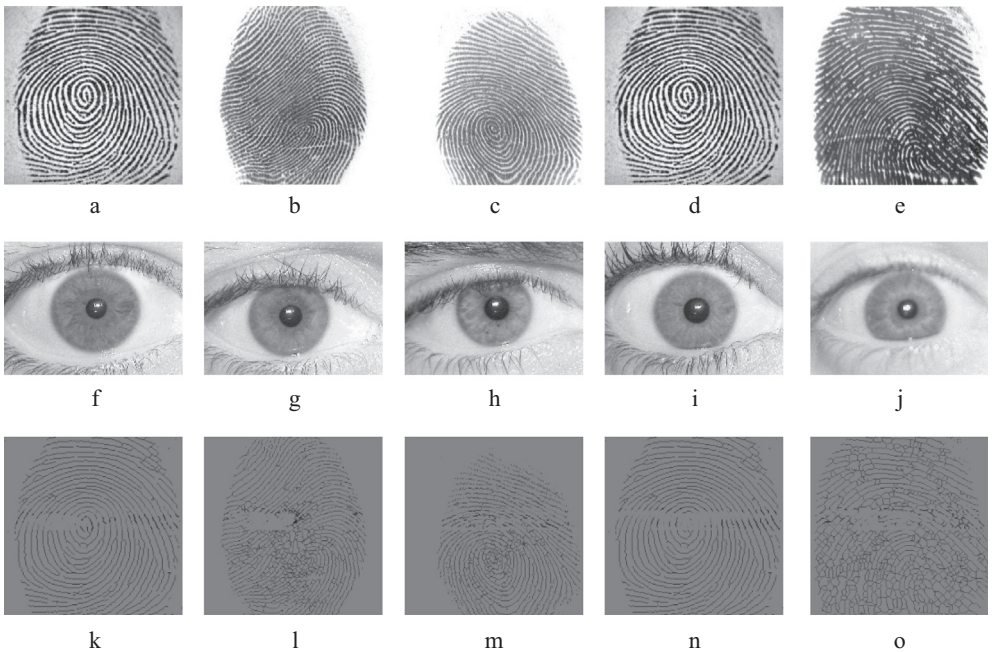

Figure 6 (a)–(e) represents input fingerprint images, (f)–(j) represents input iris images and (k)–(o) represents fused images using Laplacian pyramid.

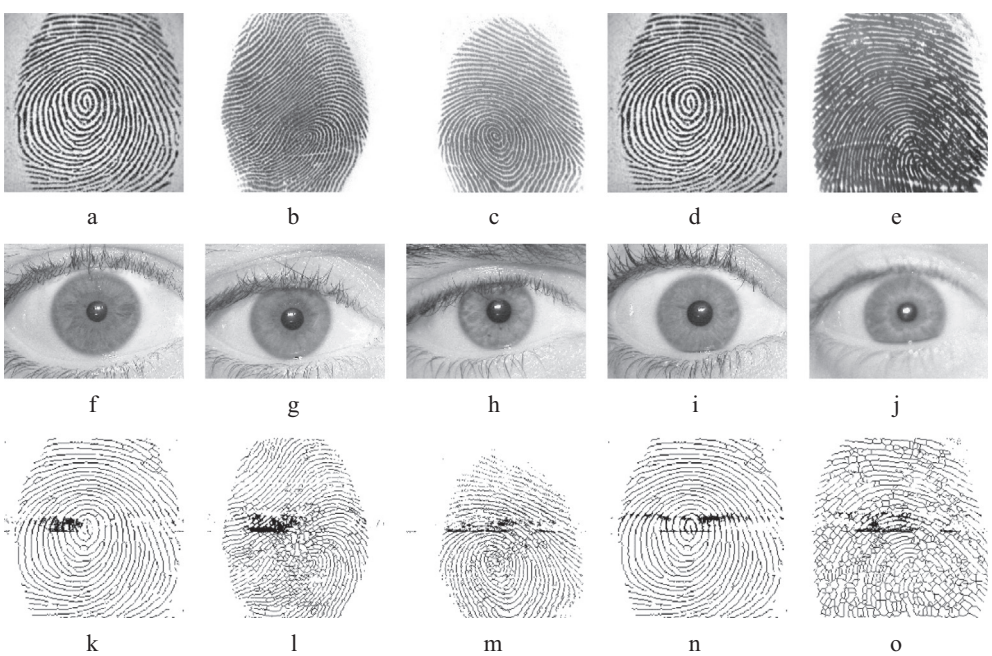

Figure 7 (a)–(e) represents input fingerprint images, (f)–(j) represents input iris images and (k)–(o) represents fused images using IHS transform.

$$VIF = \frac{\sum_k \sum_b \log_2\left(1 + \frac{g_{k,}^2 b s_{k,b}^2 C_U I}{(\sigma_{V_{k,b}}^2 + \sigma_N^2) I}\right)}{\sum_k \sum_b \log_2\left(1 + \frac{s_{k,b}^2 C_U}{\sigma_N^2 I}\right)} \tag{16}$$

The higher the value of VIF is the higher the quality of the image.

6.3. Mean Square Error and Peak Signal to Noise Ratio

The Mean Square Error (MSE) and the Peak Signal to Noise Ratio (PSNR) are the two error metrics that are used to compare image compression quality. The MSE represents the cumulative squared error between the compressed and the

original image, whereas PSNR represents a measure of the peak error. To compute the PSNR, the mean-squared error is first calculated using the following equation:

$$\mathrm{MSE} = \frac{1}{MN}\sum_{i=0}^{M-1}\sum_{j=0}^{N-1}[I(i,j) - K(i,j)]^2 \tag{17}$$

where I and K are images and M and N are the number of rows and columns in the input images, respectively. PSNR is calculated as

$$\mathrm{PSNR} = 10\log_{10}\frac{255^2}{\mathrm{MSE}} \tag{18}$$

An increase in PSNR implies high quality image and lesser the MSE value is the higher the quality of the image.

6.4. Fusion mutual information

It measures the degree of dependence of two images [26]. If the joint histogram between $I_1(x, y)$ and $I_f(x, y)$ is defined as $h_{I_1I_f}(i,j)$ and $I_2(x, y)$ and $I_f(x, y)$ are defined as $h_{I_2I_f}(i,j)$ then fused mutual information (FMI) is given as

$$FM_I = MI_{I_1I_f} + MI_{I_2I_f} \tag{19}$$

where

$$MI_{I_1I_f} = \sum_{i=1}^{M}\sum_{j=1}^{N} h_{I_1I_f}(i,j)log_2\left(\frac{h_{I_1I_f}(i,j)}{h_{I1}(i,j)h_{If}(i,j)}\right) \tag{20}$$

$$MI_{I_2I_f} = \sum_{i=1}^{M}\sum_{j=1}^{N} h_{I_2I_f}(i,j)log_2\left(\frac{h_{I_2I_f}(i,j)}{h_{I2}(i,j)h_{If}(i,j)}\right) \tag{21}$$

A large measure of fusion mutual information implies better quality.

6.5. Normalized absolute error

This gives the normalized error values between the image and fused image. It is defined as

$$\mathrm{NAE} = \sum_{j=1}^{M}\sum_{k=1}^{N}|x_{j,k} - x'_{j,k}| / \sum_{j=1}^{M}\sum_{k=1}^{N}|x_{j,k}| \tag{22}$$

The NAE value is low for better fused image.

6.6. Normalized Cross Correlation

The metric is calculated as the ratio between the net sum of the multiplication of the corresponding pixel densities of the biometric image and the fused image and the net sum of the squared values of the pixel densities of the biometric image.

The Normalized Cross Correlation value would ideally be 1 if the fused and the input images are identical.

6.7. Cross entropy

The overall cross entropy (CE) of the source images X and Y and the fused image F is

$$CE(X, Y; F) = \frac{CE(X;F) + CE(Y;F)}{2} \tag{23}$$

where $CE(X;F)$ is the cross entropy of image X and the fused image F

$$CE(X;F) = \sum_{i=0}^{L} hX(i)\log_2\frac{hX(i)}{hF(i)} \tag{24}$$

where h is the normalized histogram of image. Smaller value of cross entropy gives higher quality of fused image.

6.8. Warping degree

Warping degree represents the level of distortion of the fused image.

$$W = \frac{1}{m*n}\sum_{j=1}^{n}\sum_{i=1}^{m}|x_{ij} - xij'| \tag{25}$$

The higher the warping degree implies the higher the distortion in the image.

7. Experimental results for fusion analysis

The proposed work was implemented using Matlab7.14. For this research work, iris images are obtained from the UBIR1S.V1 database. The real-time fingerprint images of size 200×200 pixels are taken as input. The skeletonized version of the output image obtained is of size 200 x 200 pixels. Iris images of size 150×200 are taken as input. The rectangular iris image obtained is of size 64×512 pixels. Both the images are resized to 512×512 pixels and provided as inputs to the fusion technique. The output fused images are of size 512×512 pixels.

From Tables 1–3 it is inferred that the higher the values of Qabf, VIF, Mutual Information, Cross Entropy, Normalized Cross Correlation, PSNR and the lower the values of NAE and Warping Degree, DWT fusion method is better than other fusion methods.

8. Watermarking systems

8.1. DCT based watermarking

In image watermarking, a cover image is transformed by the DCT. It is usually divided into non-overlapped $N \times N$ blocks. A block that consists of 8×8 components has 64 coefficients. The watermark bit stream is embedded into eight coefficients in the lower band. For the purpose of scattering watermark into the host image and prompting security, a pseudo random system is used to generate a random position in watermarking

Table 1 Quality of fused image methods based on different metrics.

Fusion methods	Metrics		
	Qabf	VIF	Mutual information
DWT fusion	**0.45**	**0.24**	**2.71**
IHS fusion	0.33	0.13	1.74
Laplacian pyramid fusion	0.05	0.02	0.32
PCA fusion	0.26	0.12	0.77

Table 2 Quality of fused image with respect to extracted fingerprint modality.

Fusion methods	Metrics				
	CE	NAE	NCC	PSNR	Warping degree
DWT fusion	**9.75**	**0.08**	**0.98**	**13.66**	**−4.17**
IHS fusion	8.89	0.13	0.96	13.62	−2.85
Laplacian pyramid Fusion	0.39	1.20	0.45	4.79	−0.12
PCA fusion	8.05	0.16	0.903	11.85	−1.41

algorithm. The secret number is used as a seed which identifies the block to embed the watermark image.

Fig. 8 represents the flowchart for watermark embedding using DCT. Fig. 9 represents the flowchart for watermark extraction using DCT. The definition of the two-dimensional DCT for an input image A and output image B is

$$B_{pq} = \alpha_p \alpha_q \sum_{m=0}^{M-1} \sum_{n=0}^{N-1} Am, n \cos \frac{\pi(2m+1)p}{2M} \cos \frac{\pi(2n+1)q}{2N} \tag{26}$$

where p lies between 0 and $M-1$ and where q lies between 0 and $N-1$

$$\alpha_p = \begin{cases} \frac{1}{\sqrt{M}} & p = 0 \\ \sqrt{\frac{2}{M}}, & 1 \leqslant p \leqslant M-1 \end{cases} \tag{27}$$

$$\alpha_q = \begin{cases} \frac{1}{\sqrt{N}} & q = 0 \\ \sqrt{\frac{2}{M}}, & 1 \leqslant q \leqslant N-1 \end{cases} \tag{28}$$

M and N are the row and column size of A, respectively.

8.2. SVD based watermarking

The Singular Value Decomposition (SVD) is a factorization of a real or complex matrix. An A matrix can be decomposed into a product of three different matrices with SVD method. The SVD of an image A with size $m \times m$ is given by A — USV^T, where U and V are orthogonal matrices, and S = diag (λ_i) is a diagonal matrix of singular values (SV) λ_i, i = 1, …, m, arranged in decreasing order. The columns of U are the left singular vectors, whereas the columns of V are the right singular vectors of the image A. This process is known as the Singular Value Decomposition (SVD) of A, and can be written as

Table 3 Quality of fused image methods with respect to extracted iris modality.

Fusion methods	Metrics				
	CE	NAE	NCC	PSNR	Warping degree
DWT fusion	**8.21**	**0.08**	**0.98**	**20.18**	**−1.65**
IHS fusion	7.82	0.29	0.89	15.95	−1.29
Laplacian pyramid Fusion	0.08	0.68	0.43	5.26	−0.07
PCA fusion	7.63	0.40	0.81	14.09	−0.79

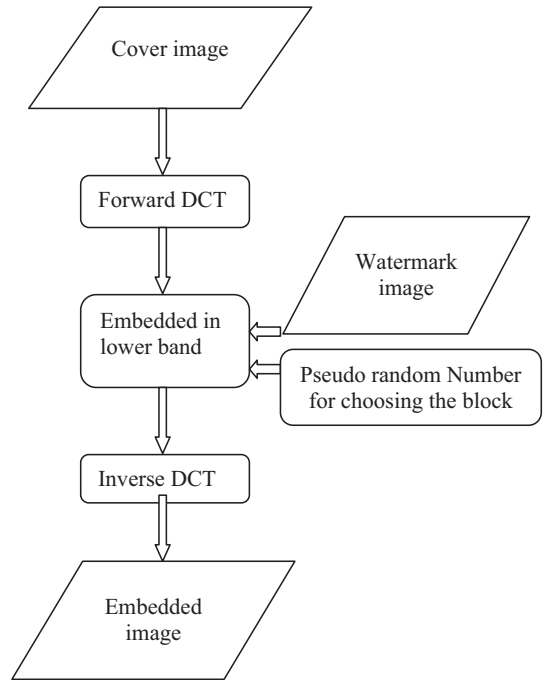

Figure 8 Flowchart for watermark embedding using DCT.

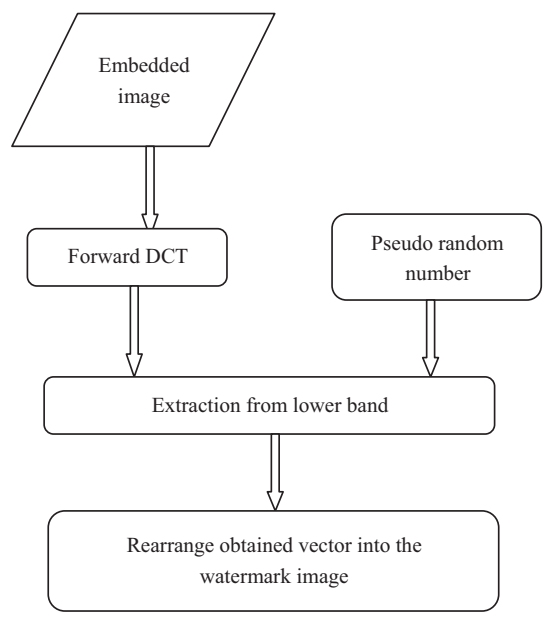

Figure 9 Flowchart for watermark extraction using DCT.

$$A = USV^T \tag{29}$$

It is important to note that each SV specifies the luminance of the image, whereas the respective pair of singular vectors specifies the intrinsic geometry properties of image. Fig. 10 represents the flowchart for watermark embedding using SVD. Fig. 11 represents the flowchart for watermark extraction using SVD. First, the SVD is employed in a cover image A to obtain U, V, and S. Second, a watermark image W is inserted into the diagonal matrix S and then apply SVD on a new matrix $S + \alpha W$ to obtain three matrices U_W, S_W, and

V_W, where α is the scaling factor which controls the intensity of the watermark to be inserted. Ultimately, the watermarked image Aw is obtained by multiplying the matrices U, S_W, and V^T.

The aforementioned three steps can be expressed by the following mathematical notions:

$$A = USV^T \tag{30}$$

$$S + \alpha W = U_W S_W V_W^T \tag{31}$$

$$A_W = US_W V^T \tag{32}$$

To extract the watermark, the SVD is applied on the watermarked image and hence the singular value of the watermarked image S_W is obtained. The S_W is further processed to yield the hidden image. These processes can be expressed as

$$A_W = US_W V^T \tag{33}$$

$$W = \frac{1}{\alpha}[S_W - S] \tag{34}$$

8.3. Bacterial foraging optimization algorithm water-marking

Bacteria search for nutrients in a manner to maximize energy obtained per unit time. Individual bacterium also communicates with others by sending signals. A bacterium takes foraging decisions after considering two previous factors. The process, in which a bacterium moves by taking small steps while searching for nutrients, is called chemotaxis and key idea of BFOA is mimicking chemotactic movement of virtual bacteria in the problem search space.

Here, the cover image is given as input to fed as the input for the algorithm. The input image is divided into 8×8 blocks equally based on the size of the image. Each block of the image is fed as the input for the Bacterial foraging algorithm. Based on the optimized values the best block of the cover image is identified where the watermark image is to be embedded. Therefore the watermarked image is produced as the output. Further the watermarked image is fed as the input for the extraction process. Finally the watermark image is extracted from the cover image. Fig. 12 depicts the structure of reversible watermarking using BFOA.

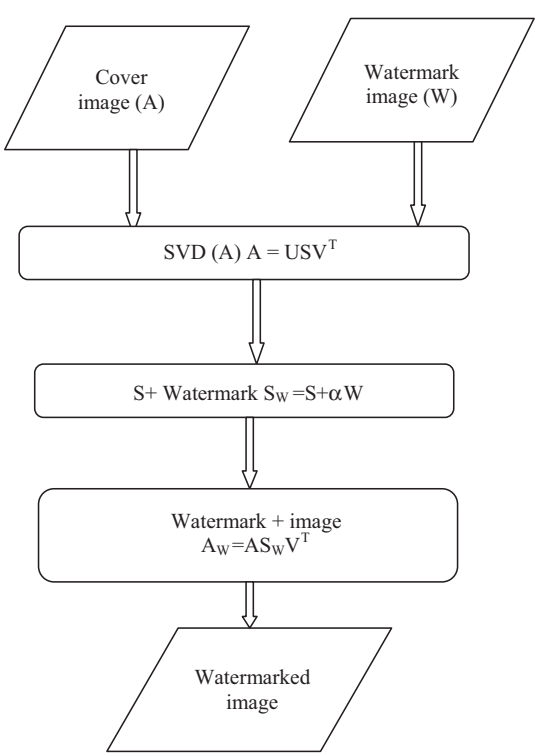

Figure 10 Flowchart for watermark embedding using SVD.

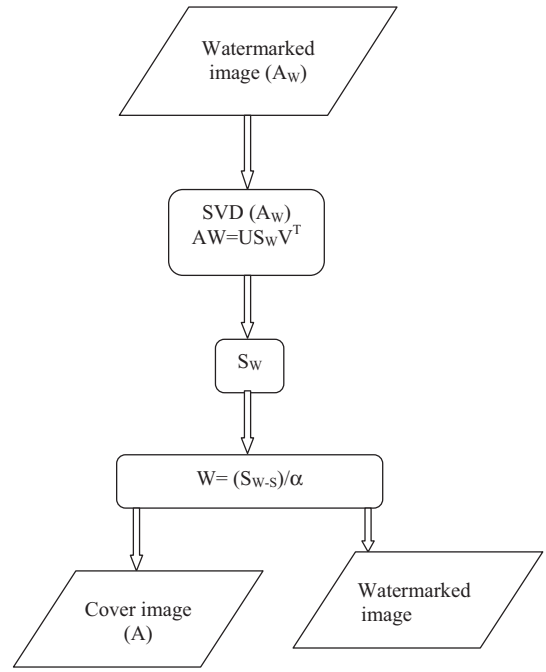

Figure 11 Flowchart for watermark extraction using SVD.

Based on the value of the fitness function, in reproduction the number of healthier values S is split into two. These are placed in the same location as their parents. Reproduction is the calculation of cumulative health of each value. Elimination and Dispersal are used to eliminate the weak values when healthy ones are added. Here, the objective function used is PSNR. Chemotaxis is used to decide the direction in which the value should move. When the maximum chemotaxis steps are reached a tumble action takes place. Based on the value of the fitness function, in reproduction the number of healthier values S is split into two. Here, the fitness function is chosen as the value of PSNR. These are placed in the same location as their parents. Reproduction is the calculation of cumulative health of each value. Elimination and Dispersal are used to eliminate the weak values when healthy ones are added.

9. Experimental results for different watermarking systems

9.1. For Baboon image

9.2. For Lena image

Figs. 13–15 represent the sample inputs and outputs of DCT, SVD and BFOA based watermarking process applied on Baboon image, and Figs. 16–18 represent the sample inputs and outputs of DCT, SVD and BFOA watermarking process applied on Lena image. Figs. 19–21 represent the performance

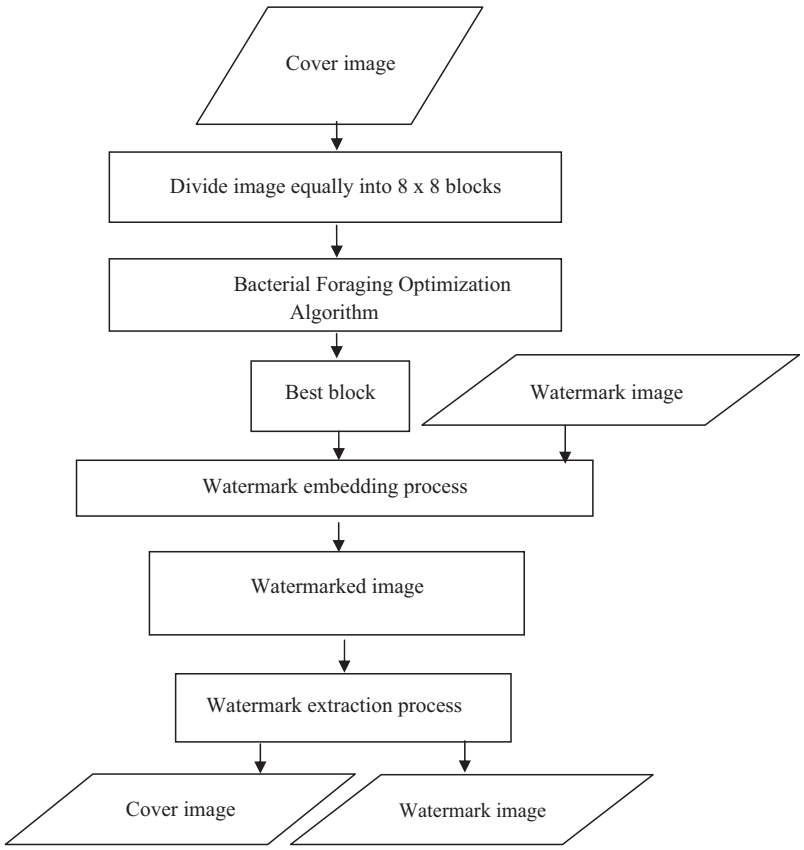

Figure 12 Flowchart for BFOA watermarking system.

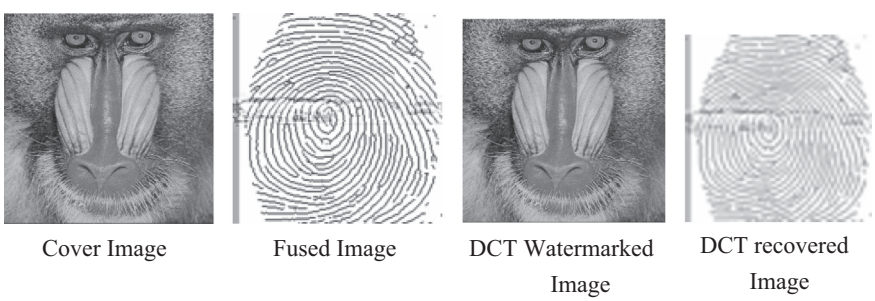

Figure 13 Sample images for DCT watermarking model using Baboon image.

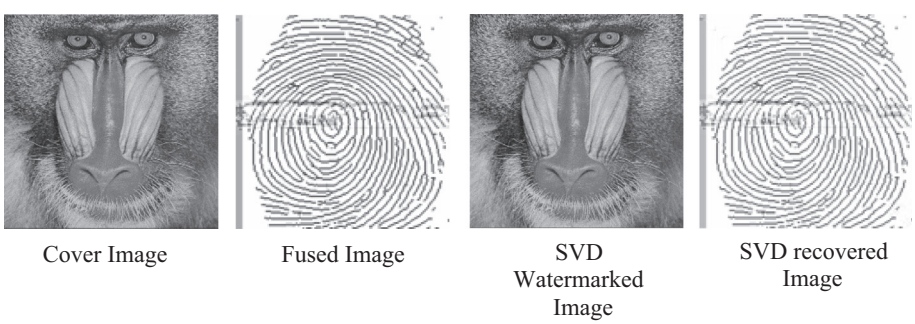

Figure 14 Sample images for SVD watermarking model using Baboon image.

Cover Image | Fused Image | BFOA Watermarked Image | BFOA recovered Image

Figure 15 Sample images for BFOA watermarking model using Baboon image.

Cover Image | Fused Image | DCT Watermarked Image | DCT recovered Image

Figure 16 Sample images for DCT watermarking model using Lena image.

Cover Image | Fused Image | SVD Watermarked Image | SVD recovered Image

Figure 17 Sample images for SVD watermarking model using Lena image.

Cover Image | Fused Image | BFOA Watermarked Image | BFOA recovered Image

Figure 18 Sample images for BFOA watermarking model using Lena image.

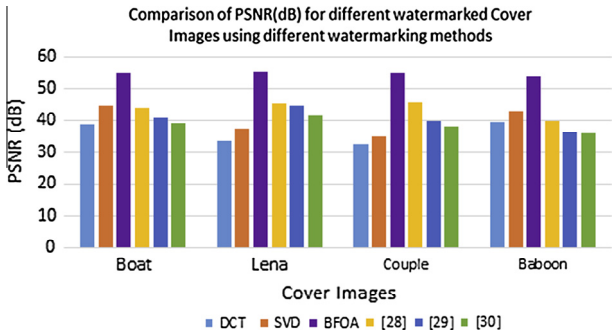

Figure 19 Performance analysis of watermarked images based on PSNR (dB) values.

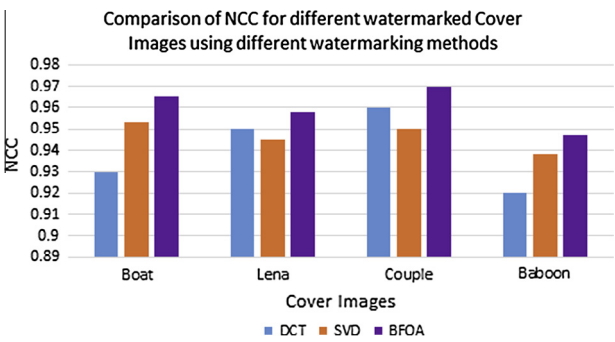

Figure 20 Performance analysis of watermarked images based on NCC values.

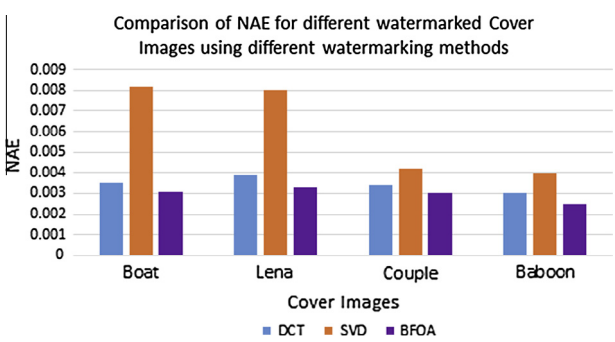

Figure 21 Performance analysis of watermarked images based on NAE values.

analysis of various watermarking systems which depicts that BFOA watermarking system performed better than other methods. The PSNR values were also compared with the watermarking methods suggested by [28–30]. The BFOA watermarking System provided better PSNR values than other watermarking systems.

10. Conclusion

The image fusion techniques and watermarking techniques are implemented using MATLAB 7.14. The fusion is performed on the input of the extracted features of fingerprint and iris. The fused images are verified using the metrics Qabf, VIF, MI, Cross entropy, Normalized Absolute error, Normalized Cross Correlation, PSNR, Mean Square Error and Warping Degree. The DWT fusion method provides better results compared to other fusion methods. Watermarking processes are analyzed by comparing the water-marked image and the original image using the quality metrics PSNR, NCC and NAE. The results indicate that BFOA watermarking system performed better than other watermarking systems.

References

[1] Ju Seung-hwan, Hee-suk Seo, Sung-hyu Han, Jae-cheol Ryou, Jin Kwak, A study on user authentication methodology using numeric password and fingerprint biometric information, BioMed Res. Int. 2013 (2013).

[2] J. Aravinth, S. Valarmathy, A novel feature extraction techniques for multimodal score fusion using density based gaussian mixture model approach, Int. J. Emerg. Technol. Adv. Eng. 2 (2012) 189–197.

[3] K. Kannan, S. Arumuga Perumal, K. Arulmozhi, Performance comparison of various levels of fusion of multi-focused images using wavelet transform, Int. J. Comput. Appl. 1 (2010) 2112–2118.

[4] Parul Shah, Shabbir N. Merchant, Uday B. Desai, An efficient adaptive fusion scheme for multifocus images in wavelet domain using statistical properties of neighborhood, in: 14th International Conference on Information Fusion, Chicago, Illinois, USA.

[5] Jyoti Sarup, Akinchan Singhai, Image fusion techniques for accurate classification of remote sensing data, Int. J. Geomat. Geosci. 2 (2011).

[6] N. Radha, A. Kavitha, Rank level fusion using fingerprint and iris biometric, Ind. J. Comput. Sci. Eng. 2 (January 2012) 917–923.

[7] Sunil Kumar Panjeta, Deepak Sharma, A survey on image fusion techniques used to improve image quality, Int. J. Appl. Eng. Res. 7 (2012) 0973.

[8] M.A.P. Maheswari, S. Ancy, EbenPraisy, K. Devanesam, Biometric identification system for features fusion of iris and fingerprint, Recent Res. Sci. Technol. 4 (2012) 308–320.

[9] Deepak Kumar Sahu, M.P. Parsai, Different image fusion techniques -a critical review, Int. J. Mod. Eng. Res. (2012) 4298–4301.

[10] V.P.S. Naidu, Bindu Elias, A novel image fusion technique using DCT based Laplacian pyramid, Int. J. Invent. Eng. Sci. 1 (2013) 1–9.

[11] Ben Wang, Jinkou Ding, Qiaoyan Wen, Xin Liao, Cuixiang Liu, Animage watermarking algorithm based on dwt, dct and svd, in: IEEE International Conference on Network Infrastructure and Digital Content, 2009, Beijing, pp. 1034–1038.

[12] F.S. Nidalb, Adham, Digital watermarking system based on cascading haar wavelet transform and dwt, J. Appl. Sci. 10 (2010) 2168–2186.

[13] Tribhuwan Kumar Tewari, Vikas Saxena, An improved and robust dct based digital image watermarking scheme, Int. J. Comput. Appl. 3 (2010).

[14] Vipul Sharma, S.S.Pattnaik, Tanuj Garg, A review of bacterial foraging optimization and its applications, in: National Conference on Future Aspects of Artificial intelligence in Industrial Automation 2012, Foundation of Computer Science, New York, USA, 9–12, May 2012, pp. 9–12.

[15] De Li, Yingying ji, Jong Weon Kim, A video watermarking scheme based on 2d dwt and pseudo 3d dct, in: International Conference on Information and Computer Applications (ICICA 2012), IACSIT Press, Chengde/China, 14–09-2012, pp. 147–150.

[16] Vidhi Khanduja, Om Prakash Verma, Shampa Chakraverty, Watermarking relational databases using bacterial foraging algorithm, Multi-Media Tools Appl. (2013).

[17] Riya Mary Thomas, Survey of bacterial foraging optimization algorithm, Int. J. Sci. Mod. Eng. (IJISME) 1 (March 2013).
[18] P. Lenarczyk, Z. Piotrowski, Parallel blind digital image watermarking in spatial and frequency domains, Telecommun. Syst. 54 (2013) 287–303.
[19] K. Loukhaoukha, M. Nabti, K. Zebbichie, A robust SVD based image watermarking using a multi-objective particle swarm optimization, Opto-Electron. Rev. 22 (2014) 45–54.
[20] Vivek Singh Verma, Rajib Kumar Jha, Improved watermarking technique based on significant difference of lifting wavelet coefficients, Signal Image Video Process. 8 (2014).
[21] Yuanning Liu, Youwei Wang, Xiaodong Zhu, Novel robust multiple watermarking against regional attacks of digital images, Multimedia Tools Appl. 68 (2014).
[22] Navneet Yadav, Kulbir Singh, Robust image-adaptive watermarking using an adjustable dynamic strength factor, Signal Image Video Process. 8 (January 2014).
[23] P.U. Lahane, S.R. Ganorkar, Efficient iris and fingerprint fusion for person identification, Int. J. Comput. Appl. 50 (2012).
[24] Shivsubramani Krishnamoorthy, K.P. Soman, Implementation and comparative study of image fusion algorithms, Int. J. Comput. Appl. 9 (2010) 25–35.
[25] FirouzAbdullah Al-Wassai, N.V. Kalyankar, Ali A. Al-Zuky, The ihs transformations based image fusion, Information Fusion 2 (2013).
[26] Nedeljko Cvejie, Artur Loza, David Bull, Nishan Canagarajah, A similarity metric for assessment of image fusion algorithms, Int. J. Inf. Commun. Eng. 2 (2006) 178–182.
[27] Yu Han, Yunze Chai, Yin Chao, Xiaming Xu, A new image fusion performance metric based on visual information fidelity, Information Fusion (2013) 127–135.
[28] B. Sikander, M. Ishtiaq, M.A Jaffar, M. Tariq, A.M. Mirza, Adaptive digital watermarking of images using genetic algorithm, in: International Conference on Information Science and Applications (ICISA), 2010, IEEE, 21–23 April 2010, pp. 1–8.
[29] A. Khan, A.M. Mirza, A. Majid, Optimizing perceptual shaping of a digital watermark using genetic programming, Iranian J. Electr. Comput. Eng. (IJECE) 3 (2004) 1251–1260.
[30] A. Khan, A.M. Mirza, A. Majid, Intelligent perceptual shaping of a digital watermark: exploiting characteristics of human visual system, Int. J. Knowledge-based Intell. Eng. Syst. (KES) 9 (2005) 1–11.